Inorganic Chemistry Communications 49 (2014) 159–162

Contents lists available at ScienceDirect

Inorganic Chemistry Communications

journal homepage: www.elsevier.com/locate/inoche

A novel porous molybdophosphate-based $Fe^{II,III}$-MOF showing selective dye degradation as a recyclable photocatalyst

Wei Zhu [a], Xiu-Yun Yang [a], Yun-Hui Li [a], Jian-Ping Li [a], Dai Wu [a], Ying Gao [a,*], Fei-Yan Yi [b,**]

[a] School of Chemistry & Environmental Engineering, Changchun University of Science & Technology, Changchun 130022, China

[b] State Key Laboratory of Rare Earth Resource Utilization, Changchun Institute of Applied Chemistry, Chinese Academy of Sciences, 5625 Renmin Street, Changchun, Jilin 130022, China

ARTICLE INFO

Article history:
Received 27 July 2014
Received in revised form 23 September 2014
Accepted 25 September 2014
Available online 26 September 2014

Keywords:
Molybdophosphate
Porous MOF
Structure
Photocatalyst
Dye degradation

ABSTRACT

A novel molybdophosphate-based $Fe^{II,III}$-metal organic framework (FeMoP-MOF) has been synthesized under hydrothermal condition and structurally characterized by elemental analysis, infrared spectroscopy, TGA, and single-crystal X-ray diffraction, namely, $\{Na_6(H_2O)_{12}[Fe^{II}_2]_2[Fe^{III}_4(PO_4)][Fe^{II}(Mo_6O_{15})_2(PO_4)_8]_2\}(OH)_3\cdot 33H_2O$ (**1**). In **1**, every four adjacent sandwich-type $Fe^{II}[P_4Mo_6O_{31}]_2$ clusters are connected into a huge secondary building unit (SBU) with a large trigonal-tapered cage by $[PO_4]$ tetrahedra, further being extended into a porous 3D framework by Fe^{II}_2 dimers with cross-shaped channels. The central 4-fold $[PO_4]$ tetrahedron spirally bridging four Fe^{III} centers resides in the cage and was connected into the SBU. The most interesting feature is that the porous framework exhibits excellent selective degradation for Rhodamine B (RhB) dye as a photocatalyst under visible light irradiation.

The design and synthesis of polyoxometalates (POMs), a typical class of metal-oxygen clusters, have received great interest not only for their potential applications in many fields ranging from catalysis, medicine to electrochemistry, etc., but also for their intriguing architectures [1–5]. Recently, POMs have been studied as green and cheap photocatalysts for the removal of organic pollutants from water [6–10], which are attributed to their unique structural features, such as oxygen-rich surfaces and high negative charges, and a number of features in common with semiconductor metal oxide clusters: (1) POMs are photostable and non-toxic; (2) POMs have similar photochemical characteristics of semiconductor photocatalysts, such as TiO_2. But TiO_2-photocatalyst is only activated by UV light due to its band gap, which limits its practical application. POMs are superior, because they have excellent redox properties and visible light-excited POMs with high oxidizing ability are able to completely degrade organic pollutants [11–19]. Organic pollutants such as various dyes in the wastewater are often from textiles, papers, leathers, food, and cosmetics, which are regarded as one of major serious worldwide problems because of their non-biodegradability, toxicity and unpleasant coloring as well as a harmful effect on the water environment. The removal of these organic pollutions has been an urgent and important task. Therefore, many researchers have attempted to develop an effective material to improve the water purification efficiency. Photocatalytic system is well known to be a desirable method for the degradation of environmental pollutants among various methods for wastewater treatment. POMs as economic and effective photocatalysts exhibit excellent photochemical activities in homogeneous reactions or heterogeneous processes. So it is essential to develop more POMs catalyst for dye waste-water treatment. In particular, porous three-dimensional and high-connected POMs are more attractive and a challengeable endeavor to broaden applications of POMs in material science [20,21]. So far, some low-dimensional structures from zero-dimensional (0D) clusters to two-dimensional (2D) layers have been reported [22,23], however, three-dimensional porous POMs are observed rarely. Most of three-dimensional POMs-based hybrids were constructed based on the metal ions and chosen POMs subunits, it is a rare and challenging issue by in-situ assembling. Based on the aforementioned considerations, we started the exploration of a new POM-based MOF by virtue of in situ assembly. Herein, we reported a new porous molybdophosphate-based $Fe^{II,III}$-metal organic framework (FeMoP-MOF) with cross-shaped channels under hydrothermal conditions, which was constructed by $Fe^{II}[P_4Mo_6O_{31}]_2$ cluster, $[Fe^{III}_4PO_4]$ tetrahedra, and $[Fe^{II}_2]$ dimers. The compound represents the first porous 3D framework in Fe–Mo–P system. The further studies have shown that it exhibits not only selective active photocatalytic for degradation of RhB under visible light irradiation, but also very stable and easily separated from the reaction system for reuse.

The compound **1** was hydrothermally synthesized by reaction of $FeCl_2$, Na_2MoO_4, H_3PO_4, and imidazole at 180 °C for 3 days [24]. In this reaction system, imidazole as a basic adjustment plays an important

* Correspondence to: Y. Gao, School of Chemistry & Environmental Engineering, Changchun University of Science & Technology, Changchun 130022, China.
** Correspondence to: F.Y. Yi, State Key Laboratory of Rare Earth Resource Utilization, Changchun Institute of Applied Chemistry, Chinese Academy of Sciences, 5625 Renmin Street, Changchun, Jilin 130022, China.
E-mail addresses: Zjw1095@sina.com (Y. Gao), fyyi@ciac.ac.cn (F.-Y. Yi).

http://dx.doi.org/10.1016/j.inoche.2014.09.033
1387-7003/

role in the synthesis of **1**, despite that it was not contained in the final structure. In additon, reaction temperature was also optimized to 180 °C for phase purity. The measured XRD pattern of the bulk material for **1** is in good agreement with the corresponding simulated pattern, demonstrating its phase purity, as shown in Fig. S1.

The single crystal X-ray analysis reveals that complex **1** crystallizes in the tetragonal space group $I4_1$/acd [25] (Table S1). As shown in Figs. 1 and 2, the structure of **1** consists of sandwich-type $\{Fe(1)^{II}[P_4Mo_6O_{31}]_2\}$ cluster (Fig. 2a), $[Fe(3)^{III}{}_4(PO_4)]$ helical blade (Fig. 1b), $[Fe(2)^{II}{}_2]$ dimer (Fig. 2c), six sodium cations, three hydroxyl anions, twelve coordinated water molecules and thirty-three lattice water molecules. Each Mo atom shows a $[MoO_6]$ octahedral environment by one terminal μ_1-O, one μ_3-O, and four μ_2-O atoms with the Mo–O distances in the ranges of 1.669(5)–2.393(4)Å (Fig. 1a, S2 and Table S2). These Mo–O values lie within the normal range [26–28]. Adjacent $[MoO_6]$ octahedra are linked into a $[P_4Mo_6O_{31}]$ ring (abbreviated as $[P_4Mo_6]$, Fig. 1a) by edge-sharing oxygen bridges from four $[PO_4]$ tetrahedra with Mo…Mo distances (2.582(1)–2.618(1) Å). The six molybdenum centers lie approximately in the same plane. The central $[P(5)O_4]$ tetrahedron bridges alternately the $[Mo_6]$ ring by μ_3-$\eta^1\eta^1\eta^1\eta^0$ oxygen atoms; each of the other three $[PO_4]$ tetrahedra containing P(2), P(3), and P(4) bridges two $[MoO_6]$ octahedra by μ_2-$\eta^1\eta^1\eta^0\eta^0$ oxygen atoms, forming a trigonal symmetry mode. $Fe(1)^{II}$ lies on an inversion center with 1/2 occupancy, bridging two $[P_4Mo_6]$ units into a sandwich-type $\{Fe(1)^{II}[P_4Mo_6O_{31}]_2\}$ (abbreviated as $[Fe^{II}(P_4Mo_6)_2]$) cluster by six edge-sharing oxygen atoms from $[MoO_6]$ octahedra, and completing an octahedral geometry. The unique P(1) lies on 4_1-fold spiral axis with 1/4 occupancy, and links four $[Fe(3)^{III}O_6]$ octahedra by its four oxygen atoms in a spirally arranged mode (abbreviated as $[Fe^{III}{}_4(PO_4)]$), at the same time, the unique $Fe(3)^{III}$ is six-coordination with five $[P(1–5)O_4]$ tetrahedra and one terminal coordinated water molecule (abbreviated as $[Fe^{III}(PO_4)_4]$) (Fig. 1c). Each of $[Fe^{III}{}_4PO_4]$ units connects four neighboring $[Fe^{II}(P_4Mo_6)_2]$ clusters into a large SBU $\{[Fe^{III}{}_4PO_4][Fe^{II}(P_4Mo_6)_2]_4\}$with a trigonal-tapered cage and resides into the cavity (Fig. 1d). Such large SBUs are further extended into 2-fold interpenetrating 3D porous framework with ellipsoid cylindrical channels (15.58(1) × 20.54(1) Å^2) (Fig. 2b). Each single net was connected to each other into the whole 3D porous framework (Fig. 2d) with cross-shaped channels by dimer $[Fe(2)^{II}{}_2]$ units (Fig. 2c). Free water molecules occupy the pores of the channels. In the $[Fe(2)^{II}{}_2]$ unit, each unique $Fe(2)^{II}$ is octahedrally coordinated by four phosphate oxygen atoms from four $[PO_4]$ tetrahedra and two coordinated water molecules, and links each other by edge sharing. Each $[Fe(2)^{II}{}_2]$ unit is connected into six $[Fe^{II}(P_4Mo_6)_2]$ clusters by six $[PO_4]$ tetrahedra to form the target framework.

The oxidation states of P, Mo, and Fe are confirmed by XPS spectra, which were carried out in the energy region of P 2p, Mo $3d_{5/2}$, Mo $3d_{3/2}$, Fe $2p_{3/2}$, and Fe $2p_{1/2}$ (Fig. S3). The peak at 132.9 eV is attributed to P^{5+} ions, the peaks at 231.9 eV and 235.0 eV are ascribed to Mo^{6+} ions. In the energy region of Fe $2p_{3/2}$, two clearly split peaks at 711.7 and 713.1 eV should be ascribed to Fe^{2+} and Fe^{3+} ions, respectively. The peak ~725 eV is very weak for Fe $2p_{1/2}$. These results are in accordance with the results of bond valence sum (BVS) calculations [29], which show that all Mo and P centers are in the oxidation states of +6 and +5, repectively, Fe(1) and for Fe(2) are in the +2 oxidation state, Fe(3) is in the +3 oxidation state (BVS results: +1.90 for Fe(1), +2.06 for Fe(2), +2.96 for Fe(3)).

TGA result indicates that compound **1** undergoes a major weight loss of 11.0% from 25 °C to 227 °C which corresponds to the losses of free water molecules (calcd. 10.1%) (Fig. 3a). Its main framework structure is stable up to 392 °C. Such high thermal stability also set a solid foundation for the further study of photocatalytic applications.

Photocatalytic activity is an attractive property of POMs for the removal of organic pollutants from water [6–10]. In the process of photocatalytic degradation by POMs, the organic dye chromophore is damaged and broken down into nonpolluting small molecules. In this work, methyl orange (MO) and rhodamine-B (RhB) as the common organic pollutant target are selected for evaluating the photocatalytic activities of compound **1** under visible light irradiation. The experiment with a typical process [30], a suspension containing **1** (20 mg) and a 100 mL dye (MO or RhB) solution was stirred in the dark for about 30 min. In the dark, there is negligible degradation of dye solution even in the presence of catalyst. Then, the visible light irradiation started under xenon-lamp irradiation. Every 30 min, 3.0 mL sample was taken out of the reactor for analysis. As illustrated in Fig. 3b, the concentration of RhB versus reaction time was plotted. It can be seen that the RhB degraded slowly at the beginning and only reaches 50% until 2 h, then rapidly degraded to achieve 100% in following 1 h. By contrast, only limited photodegradation about 10% of the MO after 3 h irradiation was observed in the presence of **1** (Fig. S4). These results imply that FeMoP-MOF (**1**) is an effective photocatalyst for RB, and shows excellent selective catalysis among RhB and MO.

The repeatability of the photocatalytic activity for the photocatalyst is a very important parameter to assess the photocatalyst practicability. Four catalyst cycles in repetitive degradation of RhB with a constant concentration in the presence of FeMoP-MOF (**1**) have been examined (Fig. S6). After each cycle of RhB degradation, the **1**-photocatalyst can be separated by simple centrifugation for its insoluble properties in

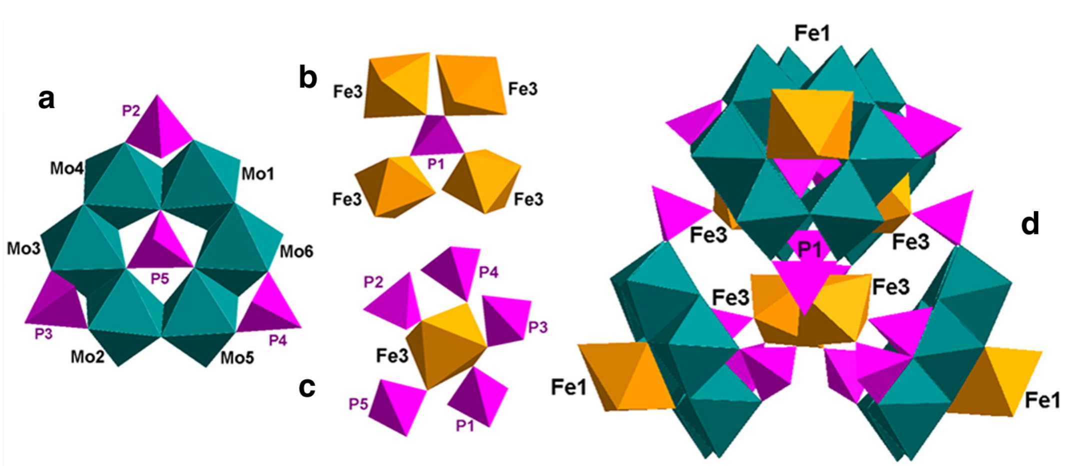

Fig. 1. The polyhedral representation of $[Mo_6O_{15}(PO_4)_4]^{6-}$ cluster abbreviated as $[P_4Mo_6]^{6-}$ (a), the central $Fe(3)^{III}{}_4P(1)$ unit (b), $Fe(3)^{III}[PO_4]_5$ unit (c) in which $Fe(3)^{III}$ octahedron are connected into five $[PO_4]$ tetrahedra, and a huge secondary building unit (SBU) (d) constructed by four adjacent $[P_4Mo_6]^{6-}$ clusters. $[MoO_6]$ and $[FeO_6]$ octahedra, and $[PO_4]$ tetrahedra are shaded in dark green, gold, and pink, respectively. (For interpretation of the references to color in this figure legend, the reader is referred to the web version of this article.)

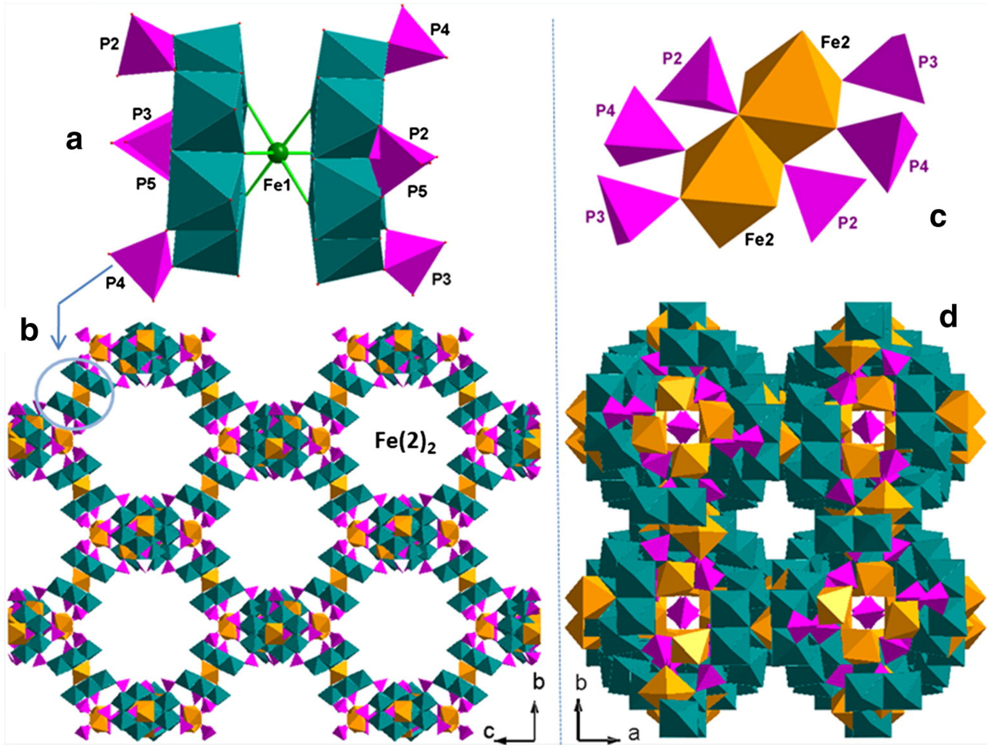

Fig. 2. (a) A sandwich-type $Fe^{II}[P_4Mo_6]_2$ cluster; (b) A 3D porous framework along [100] direction; (c) A $Fe(2)^{II}{}_2$ dimer; (d) the total 3D porous framework along [001] direction with cross-shaped channel. The free water molecules are omitted for clarity.

water, and was dried at 80 °C for 12 h, then being used next catalyst cycle. The UV–vis spectra show that **1**-catalyst did not exhibit a significant loss of activity after four cycles of photocatalytic tests. The results suggest that **1**-catalyst is considerably stable during the photodegradation of RhB. Furthermore, the PXRD pattern after each catalyst cycle also matches well with the simulated pattern generated from the result of single-crystal diffraction data and as-synthesized product (Fig. S1), indicating that the structure of FeMoP-MOF (**1**) remains intact, which also confirms its good stability. The above results illustrate the FeMoP-MOF (**1**) is reusable. In a word, the photocatalyst-**1** not only displays good photocatalytic activity under visible light irradiation, but also exhibits good reproducibility. The foregoing two aspects are of great significance for practical use of the photocatalyst.

In summary, a water-stable and insoluble photocatalyst was synthesized by in-situ hydrothermal synthesis and characterized. The compound **1** represents the first porous 3D framework with cross-shaped channel in Fe–Mo–P system. Most strikingly, the 3D compound **1** shows photocatalytic activities and can effectively degrade RhB in the visible light irradiation. In addition, it is very stable and easily recovered from the reaction system for reuse. This research may supply a new strategy for constructing the POM-based photocatalytic materials, and further encourage us to more explore the high dimensional POM systems by in-situ reaction.

Acknowledgments

This work was supported by the NSFC (21171162 and 21201162), the SRF for ROCS (State Education Ministry) and the Jilin Province Youth Foundation (20130522132JH and 20130522170JH).

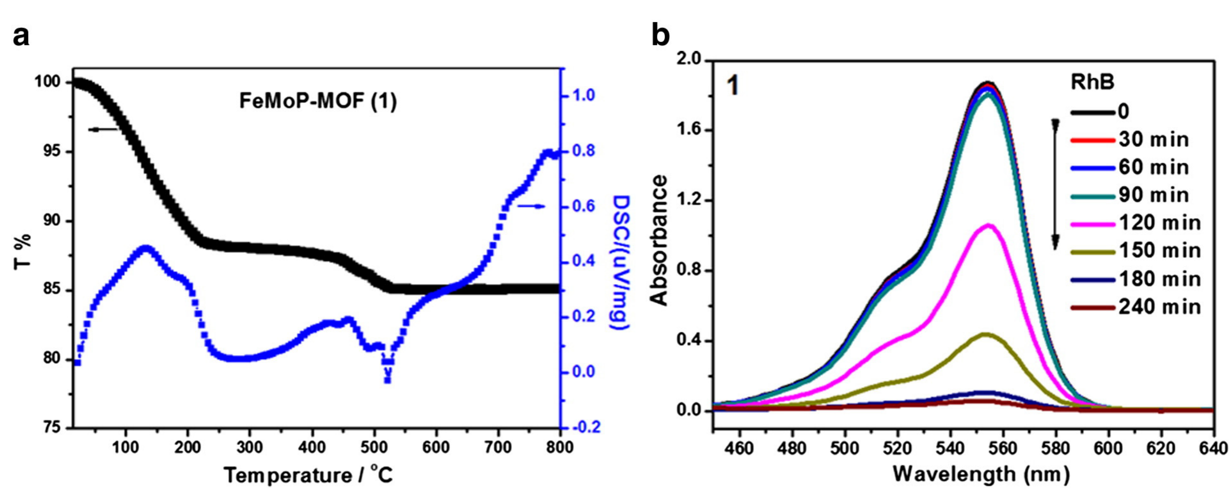

Fig. 3. (a) The TGA–DTA curves of compound **1** under air atmosphere. (b) The UV–vis spectral changes of RhB solution under visible light irradiation in different reaction time.

Appendix A. Supplementary material

Crystallographic data for compound **1** have been deposited at the Cambridge Crystallographic Data Center with the deposition number of CCDC 1015166. These data can be obtained free of charge from the Cambridge Crystallographic Data Center via www.ccdc.cam.ac.uk/conts/retrieving.html. Supplementary data associated with this article can be found, in the online version, at http://dx.doi.org/10.1016/j.inoche.2014.09.033.

References

[1] C.L. Hill, Polyoxometalates in catalysis, J. Mol. Catal. A Chem. 262 (2007) 1–242.

[2] B. Keita, L. Nadjo, Electrochemistry of polyoxometalates, in: A.J. Bard, M. Stratmann (Eds.), Encyclopedia of electrochemistry, 7, Wiley-VCH, New-York, 2006, p. 607.

[3] B. Nohra, H.E. Moll, L.M.R. Albelo, P. Mialane, J. Marrot, C. Mellot-Draznieks, M. O'Keeffe, R.N. Biboum, J. Lemaire, B. Keita, L. Nadjo, A. Dolbecq, Polyoxometalate-based metal organic frameworks (POMOFs): structural trends, energetics, and high electrocatalytic efficiency for hydrogen evolution reaction, J. Am. Chem. Soc. 133 (2011) 13363–13374.

[4] A. Dolbecq, E. Dumas, C.R. Mayer, P. Mialane, Hybrid Organic–inorganic polyoxometalate compounds: from structural diversity to applications, Chem. Rev. 110 (2010) 6009–6048.

[5] X. Kuang, X. Wu, R. Yu, J.P. Donahue, J. Huang, C.-Z. Lu, Assembly of a metal–organic framework by sextuple intercatenation of discrete adamantane-like cages, Nat. Chem. 2 (2010) 461–465.

[6] A. Dolbecq, P. Mialane, B. Keita, Louis Nadjo, Polyoxometalate-based materials for efficient solar and visible light harvesting: application to the photocatalytic degradation of azo dyes, J. Mater. Chem. 22 (2012) 24509–24521.

[7] Z.-J. Liu, S. Yao, Z.-M. Zhang, E.-B. Wang, A polyoxometalate-based ionic crystal assembly from a heterometallic cluster and polyoxoanions with visible light catalytic activity, RSC Adv. 3 (2013) 20829–20835.

[8] B.-L. Fei, W. Li, J.-H. Wang, Q.-B. Liu, J.-Y. Long, Y.-G. Li, K.-Z. Shao, Z.-M. Su, W.-Y. Sun, A novel 3D inorganic heteropoly blue as visible light responsive photocatalyst, Dalton Trans. 43 (2014) 10005–10012.

[9] Y. Hua, G. Chen, X. Xu, X. Zou, J. Liu, B. Wang, Z. Zhao, Y. Chen, C. Wang, X. Liu, Comparative study of homogeneous and heterogeneous photocatalytic degradation of RhB under visible light irradiation with Keggin-type manganese-substituted catalysts, J. Phys. Chem. C 118 (2014) 8877–8884.

[10] W.-Q. Kan, J. Yang, Y.-Y. Liu, J.-F. Ma, Inorganic–organic hybrid compounds based on octamolybdates and multidentate N-donor ligand: syntheses, structures, photoluminescence and photocatalysis, Dalton Trans. 41 (2012) 11062–11073.

[11] H. Yang, T. Liu, M. Cao, H. Li, S. Gao, R. Cao, A water-insoluble and visible light induced polyoxometalate-based photocatalyst, Chem. Commun. 46 (2010) 2429–2431.

[12] C.M. Xue, S.X. Li, L. Zhang, J.Q. Sha, T.Y. Zheng, L. Li, Hydrothermal Synthesis, Characterization and Electrocatalytic/Photocatalytic Activities of New Polyoxometalate Based Hybrid Compound, J. Inorg. Organomet. Polym 23 (2013) 1468–1476.

[13] A. Hiskia, A. Mylonas, E. Papaconstantinou, Comparison of the photoredox properties of polyoxometallates and semiconducting particles, Chem. Soc. Rev. 30 (2001) 62–69.

[14] Y.-H. Guo, C.-W. Hu, Porous hybrid photocatalysts based on polyoxometalates, J. Cluster Sci. 14 (2003) 505–526.

[15] M.T. Pope, Heteropoly and Isopoly Oxometalates, Springer-Verlag, Berlin, Heidelberg, New York, Tokyo, 1983. 1–180.

[16] C. L. Hill (Guest Ed.), Introduction: PolyoxometalatessMulticomponent Molecular Vehicles To Probe Fundamental Issues and Practical Problems, Chem. Rev. 98 (1998) 1–389.

[17] R.N. Biboum, C.P. Nanseu Njiki, G. Zhang, U. Kortz, P. Mialane, A. Dolbecq, I.M. Mbomekalle, L. Nadjo, B. Keita, High nuclearity Ni/Co polyoxometalates and colloidal TiO_2 assemblies as efficient multielectron photocatalysts under visible or sunlight irradiation, J. Mater. Chem. 21 (2011) 645–650.

[18] M. Cao, J. Lin, J. Lu, Y. You, T. Liu, R. Cao, Development of a polyoxometallate-based photocatalyst assembled with cucurbit[6]uril via hydrogen bonds for azo dyes degradation, J. Hazard. Mater. 186 (2011) 948–951.

[19] S. Kim, J. Yeo, W. Choi, Simultaneous conversion of dye and hexavalent chromium in visible light-illuminated aqueous solution of polyoxometalate as an electron transfer catalyst, Appl. Catal. B Environ. 84 (2008) 148–155.

[20] Q. Han, X. Sun, J. Li, P. Ma, J. Niu, Novel isopolyoxotungstate $[H_2W_{11}O_{38}]^{8-}$ based metal organic framework: as lewis acid catalyst for cyanosilylation of aromatic aldehydes, Inorg. Chem. 53 (2014) 6107–6112.

[21] J.-X. Meng, Y. Lu, Y.-G. Li, H. Fu, E.-B. Wang, Controllable self-assembly of four new metal–organic frameworks based on different phosphomolybdate clusters by altering the molar ratio of H_3PO_4 and Na_2MoO_4, CrystEngComm 13 (2011) 2479–2486.

[22] R. Yu, X.-F. Kuang, X.-Y. Wu, C.-Z. Lu, J.P. Donahue, Stabilization and immobilization of polyoxometalates in porous coordination polymers through host–guest interactions, Coord. Chem. Rev. 253 (2009) 2872–2890.

[23] M. Bartholomä, S. Jones, J. Zubieta, Construction of bimetallic oxide materials from molybdate building blocks and copper–ligand tethers with flexible spaces: structures of the two-dimensional $[\{Cu_2(L^4)(H_2O)_2\}Mo_8O_{26}(H_2O)_2]$ and of the three-dimensional $[\{Cu_2(L_4)\}_2(Mo_8O_{26})(MoO_4)_2]$ ($L^4 = N^1, N^1, N^4, N^4$-tetrakis(pyridin-2-ylmethyl)butane-1,4-diamine), Inorg. Chem. Commun. 14 (2011) 107–110.

[24] $\{Na_6(H_2O)_{12}[Fe^{II}{}_2]_2[Fe^{III}{}_4(PO_4)][Fe^{II}(Mo_6O_{15})_2(PO_4)_8]_2\}(OH)_3\cdot 33H_2O$ (**1**) was prepared by hydrothermal reaction of $FeCl_2\cdot 4H_2O$ (0.2 mmol, 39.7 mg), $Na_2MoO_4\cdot 4H_2O$ (0.5 mmol, 121.0 mg), H_3PO_4 (85 wt%, 3 mL), imidazole (0. 1 mmol, 6.8 mg) and deionized water (6 mL) in a 20 mL Teflon-lined stainless steel autoclave at 180 °C for 3 days. After being cooled to room-temperature, red fusiform crystals were collected by filtration and washed by water several times. Yield ~91.4 mg (71%, based on Fe). Its purity was confirmed by powder X-ray diffraction (Fig. S1). Anal. Calcd (wt %) for **1** $H_{93}Fe_{10}Mo_{24}Na_6O_{176}P_{17}$ ($Mr = 6435.23$): H, 1.46; O, 43.75. Found: H, 1.47; O, 44.01. IR data (diamond, cm^{-1}): 3424 (m), 3229 (s), 1623 (m), 1438 (w), 1195 (m), 1041 (m), 956 (s), 919 (s), 787 (m), 708 (m), 596 (m). (Fig. S5).

[25] Crystallographic data for 1: $H_{93}Fe_{10}Mo_{24}Na_6O_{176}P_{17}$, *Fw*: 6435.23, tetragonal, $I4_1/acd$, $a = b = 27.4411(4)$ Å, $c = 38.2268(15)$ Å, $\alpha = \beta = \gamma = 90°$, $V = 28785.3(13)$ Å^3, $Z = 8$, $\rho = 2.970$ mg/m^3, $\mu = 3.345$ mm^{-1}, total 86701 reflections, unique 7104, $R_1 = 0.0370$ with $I > 2\sigma(I)$, $wR_2 = 0.0879$, and GOF = 1.078. The data collection ws carried out on a Bruker Apex II CCD diffractometer with graphite monochromated Mo-Kα radiation ($\lambda = 0.71073$ Å) at 296 K. More details about the crystallographic data and structural refinement results are summarized in Table S1. Selected bond distances are given in Table S2.

[26] K. Yu, B.-B. Zhou, Y. Yu, Z.-H. Su, G.-Y. Yang, A new organic–inorganic hybrid layered molybdenum(V) cobalt phosphate constructed from $[H_{24}(Mo_{16}O_{32})Co_{16}(PO_4)_{24}(OH)_4(C_5H_4N)_2(H_2O)_6]^{4-}$ wheels and 4,4′-bipyridine linkers, Inorg. Chem. 50 (2011) 1862–1867.

[27] W.J. Chang, Y.C. Jing, S.L. Wang, K.H. Lii, Hydrothermal synthesis of a three-dimensional organic–inorganic hybrid network formed by poly(oxomolybdophosphate) anions and nickel coordination cations, Inorg. Chem. 45 (2006) 6586–6588.

[28] J.P. Wang, J.W. Zhao, P.T. Ma, J.C.L. Ma, P. Yang, Y. Bai, M.X. Li, J.Y. Niu, A novel type of heteropolyoxoanion precursors $\{[Ca(H_2O)]_6[P_4M_6O_{34}]_2\}^{12-}$ ($M = W^{VI}, Mo^{VI}$) constructed by two $[P_4M_6O_{34}]^{12-}$ subunits via a rare hexa-calcium cluster, Chem. Commun. (2009) 2362–2364.

[29] D. Brown, D. Altermatt, Acta Crystallogr. B Struct. Sci. 41 (1985) 244.

[30] Photocatalytic reaction was carried out in a PLS-SXE 300C Xe lamp (Beijing PerfectLight Co. Ltd., China), which was placed 15 cm above the reactor. The powdered catalyst (20 mg) was dispersed in fresh aqueous solution of RhB or MO (100 mL, 5 mg L^{-1}) with a 200 mL quartz reactor, which was magnetically stirred in the dark for at least 30 min before irradiation. Subsequently, the light source was turned on, and a series of aqueous solutions of a certain volume were collected and separated through centrifuge to remove suspended catalyst particles after a regular interval visible light irradiation. The upper clear solution was analyzed by a UV–visible spectrophotometer.